I&EC research
Industrial & Engineering Chemistry Research

Article

pubs.acs.org/IECR

# Novel RGO-$ZnWO_4$-$Fe_3O_4$ Nanocomposite as an Efficient Catalyst for Rapid Reduction of 4-Nitrophenol to 4-Aminophenol

Mohamed Jaffer Sadiq Mohamed and Krishna Bhat Denthaje*

Department of Chemistry, National Institute of Technology Karnataka Surathkal, Mangalore 575025, India

Supporting Information

**ABSTRACT:** We report herein a simple, economic, and facile approach for the synthesis of a novel reduced graphene oxide-zinc tungstate-iron oxide (RGO-$ZnWO_4$-$Fe_3O_4$) nanocomposite by a one-pot microwave method and its efficiency as a catalyst in reducing 4-nitrophenol (4-NP) to 4-aminophenol (4-AP) using sodium borohydride ($NaBH_4$). The as-prepared RGO-$ZnWO_4$-$Fe_3O_4$ nanocomposites were characterized by X-ray diffraction (XRD), field emission scanning electron microscopy (FESEM), transmission electron microscopy (TEM), Fourier transformed infrared spectroscopy (FTIR), Raman spectroscopy, and X-ray photoelectron spectroscopy (XPS) techniques. The prepared nanocomposites showed excellent catalytic performance in the reduction of 4-NP to 4-AP. The reaction was completed in just 40 s at room temperature. The RGO in RGO-$ZnWO_4$-$Fe_3O_4$ nanocomposite plays an essential role to improve the catalytic performance through facilitation of easy electron transfer and high adsorption of the substrate on graphene sheets. The synergistic effects of RGO, $ZnWO_4$, and $Fe_3O_4$ in the RGO-$ZnWO_4$-$Fe_3O_4$ nanocomposite toward reduction, apart from its excellent stability and reusability, make it an efficient candidate as catalyst for hydrogenation reactions of aromatic compounds in research and industrial applications.

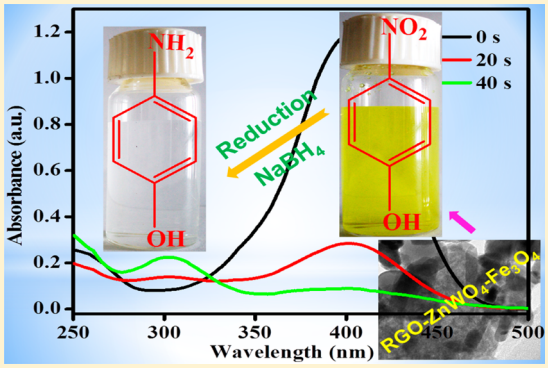


## 1. INTRODUCTION

Over the years, nanoparticles have become a class of highly sought after materials for a host of applications due to their extraordinary physicochemical properties.[1,2] One of the important areas wherein nanoparticles are being extensively used is catalysis. Metal nanoparticles possess higher Fermi potential due to which the reduction potential value is lowered in reactions. By virtue of this property, metal nanoparticles can function as efficient catalysts for a variety of electron transfer reactions.[3] Although there are a large number of metal catalysts for a good number of processes, there is still a need to develop high-performance, cost-effective, eco-friendly, and noble metal free catalysts which are more efficient, stable, earth-abundant, and reusable.[4]

Tungstate materials have been well-investigated over the past decades because of their significant and interesting industrial applications in several fields.[5] Recently, tungstates have been used as catalysts for the oxidation of benzyl chlorides, bromides, and alcohols with hydrogen peroxide. These catalysts have received substantial consideration and appreciation due to their superior property and have also been projected to be promising candidates in future commercial applications.[6−8]

Compositing of metal oxide nanomaterials with graphene has become a current method for improving heterogeneous catalytic performance for dissimilar organic reactions in pharmaceutical and chemical industries, including cross-coupling reactions, propylene epoxidation, hydrogenation reactions, reduction of 4-NP to 4-AP, oxidation of alcohols, etc.[9−11] Specifically, the reduction of 4-NP on metal oxide-graphene in the presence of $NaBH_4$ has been mostly studied in the manufacture of 4-AP, which is a well-known intermediate in the synthesis of antipyretic and analgesic drugs.[12,13] 4-AP is widely used as an anticorrosion-lubricant, corrosion inhibitor, hair-dyeing agent, and photographic developer.[14,15]

To the best of our knowledge, there are no reports on RGO-$ZnWO_4$-$Fe_3O_4$ nanocomposites as heterogeneous catalyst for the reduction of aromatic nitro compounds. Herein, we report a fast, simple, and facile approach for the synthesis of novel RGO-$ZnWO_4$-$Fe_3O_4$ nanocomposites via microwave route. The nanocomposite has been characterized by X-ray diffraction, microscopic, and spectroscopic techniques for the structural, morphological, and elemental composition determination. The catalytic activity of the catalyst has been studied for the conversion of 4-NP to 4-AP in the presence of $NaBH_4$.

## 2. EXPERIMENTAL SECTION

**2.1. Materials.** Natural graphite powders were purchased from Sigma-Aldrich. All other chemicals were procured from Merck Ltd. and were used without further purification. All the experiments were performed using Millipore water.

**Received:** May 16, 2016
**Revised:** June 24, 2016
**Accepted:** June 24, 2016
**Published:** July 5, 2016





DOI: 10.1021/acs.iecr.6b01882
Ind. Eng. Chem. Res. 2016, 55, 7267−7272

**2.2. Synthesis of RGO-$ZnWO_4$-$Fe_3O_4$ Nanocomposites.** Graphene oxide (GO) was synthesized by the modified Hummers method[16] (Supporting Information). RGO-$ZnWO_4$-$Fe_3O_4$ nanocomposite was synthesized by a one-step microwave irradiation method (Figure 1). A specified amount

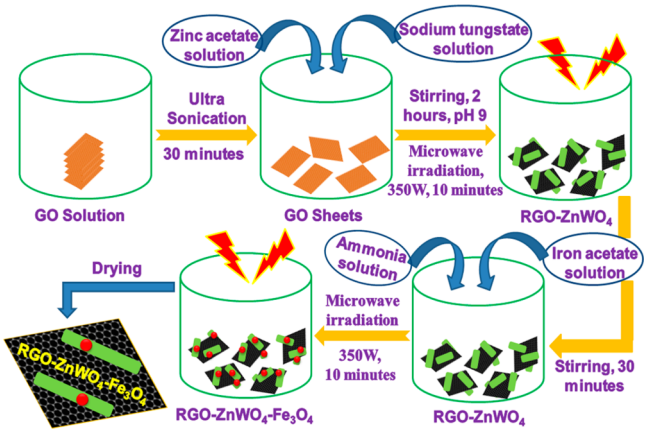


**Figure 1.** Schematic illustration of the synthesis procedure for RGO-$ZnWO_4$-$Fe_3O_4$ nanocomposite.

of GO was dispersed in ethylene glycol with ultrasonic treatment for about 30 min. A 0.05 M of zinc acetate and sodium tungstate solution was added slowly to the above dispersed GO solution under magnetic stirring for about 2 h, and to maintain a pH of 9, ammonia was used. The mixture was cooled down to room temperature after treatment with microwave irradiation (350 W) for 10 min. The precipitate of RGO-$ZnWO_4$ was obtained. Under stirring conditions, 0.01 M iron acetate and 10 mL of ammonia were added to the above mixture. After 30 min, the reaction mixture was again treated with microwave irradiation at 350 W for an additional 10 min. The obtained RGO-$ZnWO_4$-$Fe_3O_4$ precipitate was washed with 10% ethanol several times. Finally, the samples were dried in a vacuum oven at 80 °C for 12 h.

**2.3. Catalytic Study.** A 2.7 mL portion of 0.1 mM of 4-NP was mixed with 0.3 mL of 0.1 M $NaBH_4$ solution under constant magnetic stirring followed by addition of 0.1 mg of catalyst. The reduction reaction of 4-NP was investigated using UV−vis absorption spectroscopy in the range 250−500 nm. The recovery of the catalyst was done as follows. Once the reaction was completed, the catalyst was separated by ultracentrifugation. The catalyst was then thoroughly washed with 10% ethanol solution followed by vacuum drying at 60 °C for 6 h. The catalyst was then reused for subsequent cycles to study its stability and reusability.

**2.4. Characterization.** The surface morphology of the samples was obtained using SEM (JEOL) and FESEM (Zeiss Ultra 55 at an operating voltage of 200 kV). TEM and HRTEM images were obtained using a Tecnai G2-20 instrument, operated at a voltage of 120 kV. The composite samples were dispersed in pure ethanol, drop-casted onto a carbon coated Cu grid, and subsequently dried at ambient temperature overnight. The surface elemental analysis of the as-synthesized samples was done on an XPS model, Multilab 2000 (Thermo Scientific, U.K.). Binding energy values were calibrated according to the reference binding energy of the C 1s peak (C 1s 284.8 eV). The structural properties were determined using an XRD technique (Rigaku, Japan, equipped with nickel filtered Cu K$\alpha$ irradiation of 0.154 nm at a scan rate of 1° per minute in the spectral range of 5−70°). Absorbance spectra were recorded using UV−vis spectrophotometer from Analytik Jena.

## 3. RESULTS AND DISCUSSION

**3.1. Structural Analysis.** The phase structure and purity of the RGO-$ZnWO_4$-$Fe_3O_4$ nanocomposites have been examined by XRD studies. The powder pattern obtained is shown in Figure 2. The diffraction peaks could be indexed to the

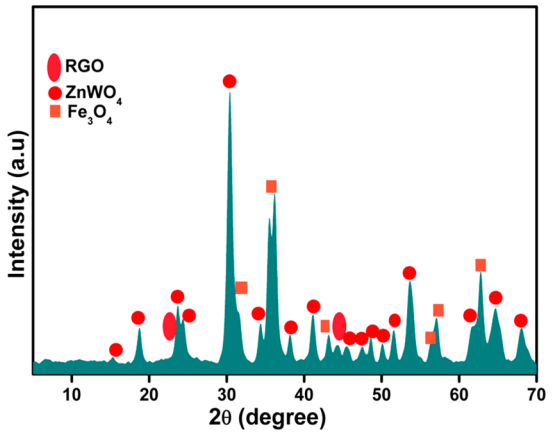


**Figure 2.** XRD pattern of RGO-$ZnWO_4$-$Fe_3O_4$ nanocomposites.

monoclinic sanmartinite phase (JCPDS card 15-0774) of $ZnWO_4$, with space group $P2/c$ (No. 13) with lattice parameter $a$ = 4.691 Å, $b$ = 5.720 Å, $c$ = 4.925 Å, and $\beta$ = 90.64°; and cubic magnetite phase (JCPDS card 19-0629) of $Fe_3O_4$ with space group $Fd\bar{3}m$ (No. 227) with lattice parameter $a$ = 8.396 Å. The diffraction peaks of RGO detected at 22.6° and 42.6° were ascribed to (002) and (100). No impurity peaks were detected suggesting the high purity of the synthesized compound. The above results show that $ZnWO_4$ and $Fe_3O_4$ particles were well-decorated on RGO successfully.

**3.2. Morphology Studies.** Electron microscope images of nanocomposites are shown in Figure 3. The images reveal the distribution of $ZnWO_4$ nanorods and $Fe_3O_4$ nanospheres anchored on the surface of the RGO nanosheets in the

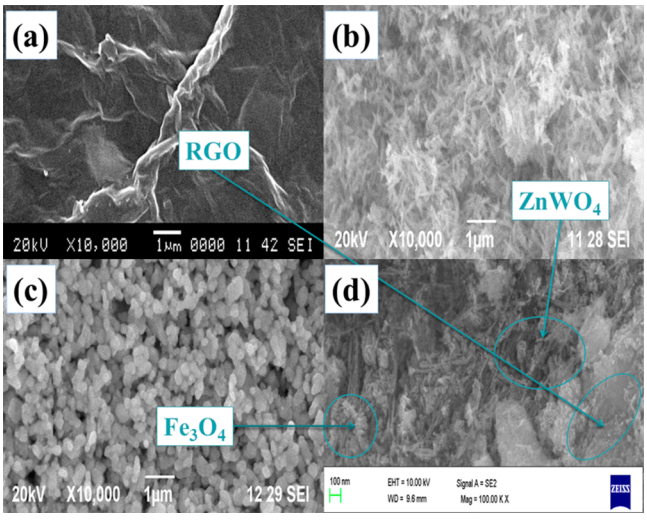


**Figure 3.** SEM images of (a) RGO, (b) $ZnWO_4$, (c) $Fe_3O_4$, and (d) RGO-$ZnWO_4$-$Fe_3O_4$ nanocomposites.



DOI: 10.1021/acs.iecr.6b01882
Ind. Eng. Chem. Res. 2016, 55, 7267−7272

nanocomposite. The morphological features of the components of the nanocomposite can be further verified by the TEM images (Figure 4). Then, the lattice fringes in the HRTEM of

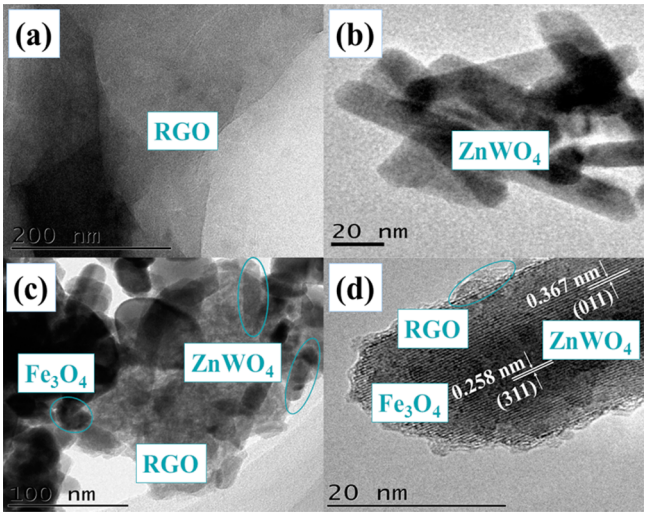


**Figure 4.** TEM images of (a) RGO, (b) $ZnWO_4$, and (c) RGO-$ZnWO_4$-$Fe_3O_4$. (d) HRTEM image of RGO-$ZnWO_4$-$Fe_3O_4$ nanocomposites.

the nanocomposite can be assigned to the (011) plane of $ZnWO_4$ (0.367 nm) and to the (311) plane of $Fe_3O_4$ (0.258 nm). Thus, it is further evident that the interface is formed by the $Fe_3O_4$ (311) plane and the $ZnWO_4$ (011) plane on the surface of the RGO sheets.

**3.3. FTIR Analysis.** FTIR spectra of RGO-$ZnWO_4$-$Fe_3O_4$ nanocomposites are shown in Figure S1. The absorption band at 588 $cm^{-1}$ corresponds to symmetric deformations of W—O in the $WO_6$ octahedron structure.[17] The band at 722 $cm^{-1}$ can be indexed to symmetrical vibration of bridged O atoms of the Zn—O—W.[18] The absorption bands at 823 and 891 $cm^{-1}$ are due to the vibration of the $WO_2$ units in the $W_2O_8$ group.[18] The bands at 554 and 638 $cm^{-1}$ can be ascribed to the intrinsic stretching vibration of Fe—O at tetrahedral structures.[19] Further, two absorption bands at 1625 and 3446 $cm^{-1}$ can be attributed to bending and stretching vibrations of H—O—H and O—H corresponding to surface adsorbed water molecules on $ZnWO_4$ and $Fe_3O_4$, respectively.[19,20] In the spectra of RGO, the broad bands centered at 1202 $cm^{-1}$ can be attributed to the C—O stretching vibration of the carboxylic groups from the reduced GO sheets.[21] Moreover, the broad band at 1563 $cm^{-1}$ corresponding to the C=C skeletal vibration from RGO sheets can be support for reduction of GO to RGO sheets.[22]

**3.4. Raman Studies.** Further structural information on the as-prepared RGO-$ZnWO_4$-$Fe_3O_4$ nanocomposites is obtained from Raman spectroscopy (Figure 5). The D and G band peaks of GO appear at 1349 and 1604 $cm^{-1}$, respectively, with an $I_D/I_G$ intensity ratio of 0.98. The same for RGO are at 1347 and 1600 $cm^{-1}$, and the $I_D/I_G$ intensity ratio is 1.10. The variation of $I_D/I_G$ intensity ratio from GO to RGO is related to the elimination of functional groups and formation of defects along with the recovery of $sp^2$ conjugated carbon structure for the duration of the reduction of GO into RGO sheets.[23] The Raman spectra of RGO-$ZnWO_4$-$Fe_3O_4$ nanocomposites exhibit the D and G bands at 1348 and 1601 $cm^{-1}$, with an $I_D/I_G$ intensity ratio of 1.03 which is slightly lower than the RGO sheets. This decrease in ratio can be attributed to the

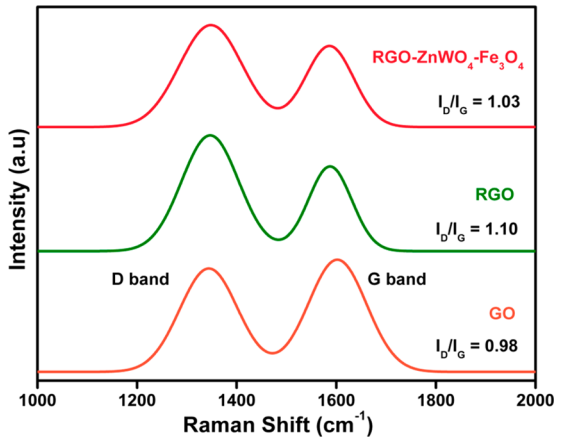


**Figure 5.** Raman spectra of GO, RGO, and RGO-$ZnWO_4$-$Fe_3O_4$ nanocomposites.

noncovalent $\pi-\pi$ interactions of nanoparticles on the RGO nanosheets.[24]

**3.5. Elemental Analysis.** The elemental states of ions present in the nanocomposites were studied through XPS analysis (Figure 6). Figure 6a shows the high-resolution C 1s spectra which could be deconvoluted into four different peaks with binding energies of 284.8, 286.6, 288.1, and 290.1 eV. These peaks are assigned to C—C/C=C bonds within the aromatic ring of $sp^2$, C—O, C=O, and O—C=O bonds in the oxygenated functional groups, respectively. Further, the intensity of the oxygenated peaks is much reduced compared to that of C—C/C=C bonds indicating that GO has been well-reduced to graphene sheets.[25] Figure 6b presents the high-resolution Zn 2p region with two broad peaks at 1019.1 and 1041.9 eV. They are allotted to Zn $2p_{3/2}$ and Zn $2p_{1/2}$ state, respectively.[26] Figure 6c shows the high-resolution W 4f spectra which could be deconvoluted into two peaks at 36.8 and 38.8 eV. The peaks can be ascribed to W $4f_{7/2}$ and W $4f_{5/2}$, respectively.[27] These results are in conformation with that of $ZnWO_4$ values reported in the literature.[28] Figure 6d shows the high-resolution Fe 2p region with two photoelectron peaks at 709.2 and 723.5 eV which correspond to Fe $2p_{3/2}$ and Fe $2p_{1/2}$, respectively.[29] These results confirm the successful incorporation of $ZnWO_4$ and $Fe_3O_4$ nanoparticles on RGO sheets and in turn the formation of RGO-$ZnWO_4$-$Fe_3O_4$ nanocomposite.

**3.6. Hydrogenation Studies.** The catalytic activity of the as-prepared RGO-$ZnWO_4$-$Fe_3O_4$ nanocomposites in reduction of 4-NP to 4-AP by $NaBH_4$ is estimated in an aqueous medium. The reduction reaction does not proceed in the absence of the catalyst. This is indicated by the undeterred absorption peak at 400 nm. However, when RGO-$ZnWO_4$-$Fe_3O_4$ nanocomposite was added into the 4-NP solution, the absorption of 4-NP found at 400 nm peak decreased immediately, and a new absorption peak of 4-AP at 300 nm was obtained. This new peak increased in the intensity with time as shown in Figure 7. The catalytic reduction of 4-NP into 4-AP was over within just 40 s. The completeness of the reaction is indicated by the reduction of the absorbance of the solution at 400 nm to zero and also by the change in color of the solution from bright yellow to colorless[30] (Figure 7). For comparison, the catalytic activities of the individual components of the composite in terms of pseudo-first-order rate constants have also been determined under identical conditions (Table S1). As can be seen from the table, the catalytic efficiency of the RGO-


DOI: 10.1021/acs.iecr.6b01882
Ind. Eng. Chem. Res. 2016, 55, 7267−7272

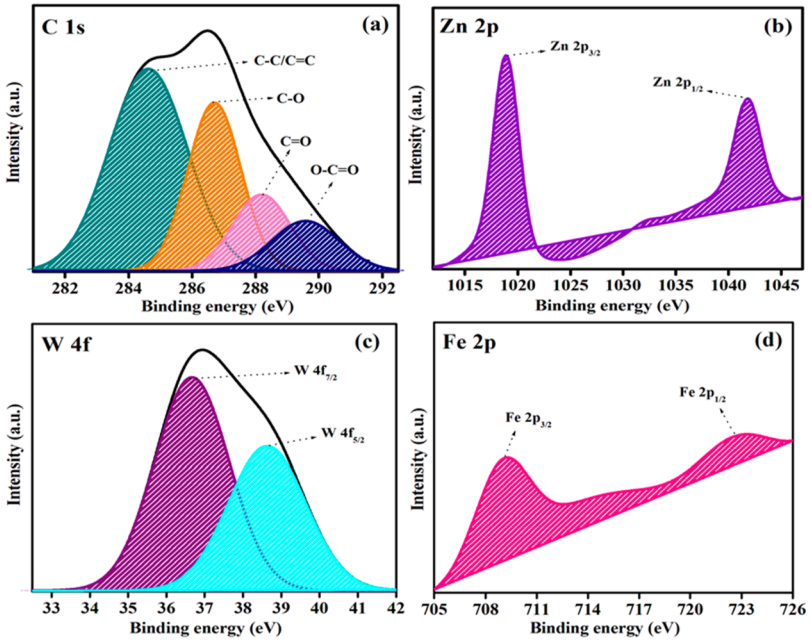


**Figure 6.** High-resolution XPS spectra of (a) C 1s, (b) Zn 2p, (c) W 4f, and (d) Fe 2p.

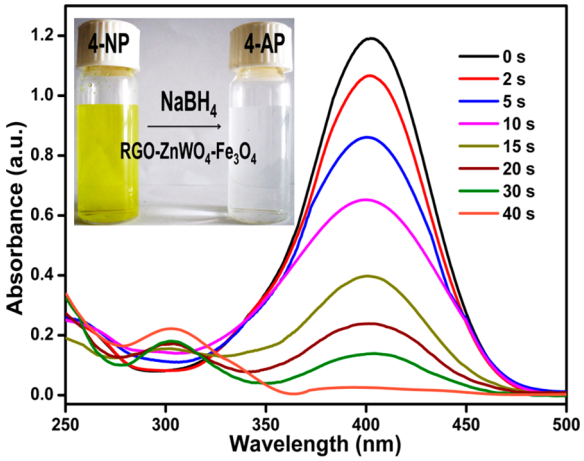


**Figure 7.** UV−vis absorption spectra for the reduction of 4-NP to 4-AP by $NaBH_4$ in the presence of RGO-$ZnWO_4$-$Fe_3O_4$ nanocomposite.

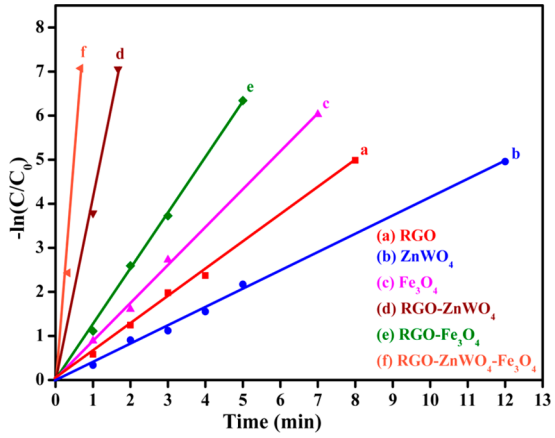


**Figure 8.** Plots of $-\ln(C/C_0)$ against the reduction time of 4-NP to 4-AP catalyzed by (a) RGO, (b) $ZnWO_4$, (c) $Fe_3O_4$, (d) RGO-$ZnWO_4$, (e) RGO-$Fe_3O_4$, and (f) RGO-$ZnWO_4$-$Fe_3O_4$.

$ZnWO_4$-$Fe_3O_4$ nanocomposite is more than that of the other component materials.

The reaction rate constants conforming to the pseudo-first-order kinetics with respect to 4-NP concentration have been determined (Figure 8). The reaction appears independent of the concentration of $BH_4^-$; the rates of the reaction mixture are assumed to have pseudo-first-order kinetics with regard to 4-NP concentration, and the same could be used to evaluate the catalytic rate. The reaction kinetics can be described as $-\ln(C/C_0) = kt$, where $k$ is the rate constant at a given temperature and $t$ is the reaction time. $C_0$ and $C$ are the 4-NP concentration at the beginning and at time $t$, respectively. The plot of $-\ln(C/C_0)$ versus time shows a straight line with a positive slope to evaluate the rate constant that was obtained in Figure 8. The kinetic rate constant ($k$) values and the catalyst activity parameter[31] ($K_a$) of the composite materials have also been calculated from the ratio of rate constants for the catalysts to the amount of given catalyst added, where $K_a = k/m$, given in Table S1. It is interesting to note the differences in the efficiencies of various catalysts. Individually, the activity of iron oxide is more than two times that of zinc tungstate. This may be due to higher catalytically active sites on iron oxide. However, with RGO, activity of zinc tungstate is more than three times that of RGO-$Fe_3O_4$. This may be due to the ease of electron transportation that is possible with RGO-$ZnWO_4$ combination compared to that of RGO-$Fe_3O_4$. Finally, when iron oxide is combined with RGO-$ZnWO_4$, the activity of the resulting nanocomposite is more than 2.5 times that of RGO-$ZnWO_4$. Evidently, the observation is due to the synergic contribution of all the components of the nanocomposite toward the catalytic process. Further, it is worth noting that the observed activity of the present catalyst is much higher compared to that for reported catalysts.[9,32−34]

The stability and reusability of the RGO-$ZnWO_4$-$Fe_3O_4$ nanocomposites were examined by carrying out the reduction reaction with the same catalyst after recovery from the previous reaction mixture. The results from 10 such successive reactions are shown in Figure 9. The reused catalyst exhibited excellent



DOI: 10.1021/acs.iecr.6b01882
Ind. Eng. Chem. Res. 2016, 55, 7267−7272

activity even after 10 successive cycles, with nearly 100% conversion within a time period of 60 s.

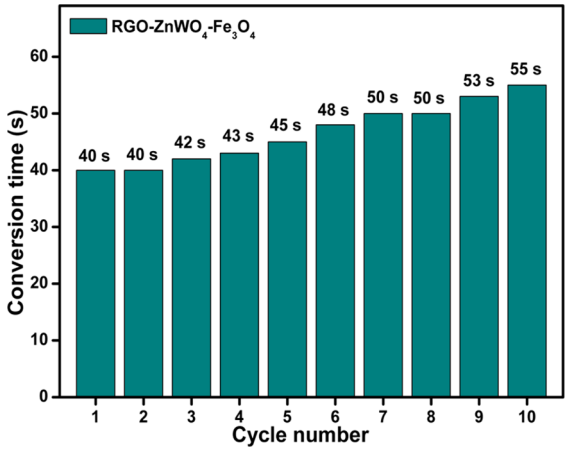


**Figure 9.** Catalytic stability of RGO-$ZnWO_4$-$Fe_3O_4$ nanocomposites with 10 successive cycles of the same reduction condition.

The possible mechanism for reduction of 4-NP to 4-AP by $NaBH_4$ in the presence of RGO-$ZnWO_4$-$Fe_3O_4$ nanocomposite catalyst may be explained as follows. The 4-NP molecule being slightly acidic can be adsorbed on to the catalyst surface to a better extent because of the fact that the RGO provides a slightly negatively charged surface. Further, the presence of $ZnWO_4$ nanoparticles on the RGO surface not only provides better active sites for adsorption but also facilitates effective interaction among the substrate, reducing agent, and catalyst matrix. This property is further enhanced by the presence of $Fe_3O_4$ nanoparticles in the nacomposite catalyst. This is also supported by the enhancement in the rate of reduction reaction observed (Figure 8) when $Fe_3O_4$ is added to the RGO-$ZnWO_4$ nanocomposite. Also, the ease of electron transfer over RGO matrix makes it an ideal mediator for reduction process and enables the acceptance of electrons by 4-NP molecules and its conversion to 4-AP. Overall, the combination of RGO, $ZnWO_4$, $Fe_3O_4$ in the RGO-$ZnWO_4$-$Fe_3O_4$ nanocomposite provides favorable synergetic effects to the complete and rapid catalytic reduction of 4-NP to 4-AP by $NaBH_4$. Further, the RGO-$ZnWO_4$-$Fe_3O_4$ nanocomposite also exhibits excellent reusability and stability for reduction processes. Hence, the RGO-$ZnWO_4$-$Fe_3O_4$ nanocomposites have great potential to be the high-performance catalysts for practical applications.

## 4. CONCLUSIONS

In summary, we have synthesized a novel RGO-$ZnWO_4$-$Fe_3O_4$ nanocomposite by a simple microwave irradiation method. The resulting RGO-$ZnWO_4$-$Fe_3O_4$ nanocomposite possesses outstanding catalytic activity in the reduction of 4-NP to 4-AP in the presence of $NaBH_4$ which is completed within 40 s. The catalyst shows good stability, recyclability, and high catalytic performance due to its synergistic chemical adsorption and electron transfer effects. We believe that a novel RGO-$ZnWO_4$-$Fe_3O_4$ nanocomposite would be a possible potential candidate as catalyst for hydrogenation of nitro compounds and other processes.

## ■ ASSOCIATED CONTENT

### Supporting Information

The Supporting Information is available free of charge on the ACS Publications website at DOI: 10.1021/acs.iecr.6b01882.

Methods; FTIR spectra of RGO, $ZnWO_4$, $Fe_3O_4$, and RGO-$ZnWO_4$-$Fe_3O_4$ nanocomposites (Figure S1); and rate constant and catalyst activity parameter of different types of catalysts (Table S1) (PDF)

## ■ AUTHOR INFORMATION

### Corresponding Author

*E-mail: denthajekb@gmail.com. Tel.: +91-824-2473202. Fax: +91-824-2474033.

### Notes

The authors declare no competing financial interest.

## ■ ACKNOWLEDGMENTS

M.J.S.M. is grateful to National Institute of Technology Karnataka—Surathkal, for the award of an Institute Research Fellowship.

## ■ REFERENCES

(1) Hu, X.; Dong, S. Metal Nanomaterials and Carbon Nanotubes-Synthesis, Functionalization and Potential Applications Towards Electrochemistry. *J. Mater. Chem.* **2008**, *18*, 1279.

(2) Ray, P. C. Size and Shape Dependent Second Order Nonlinear Optical Properties of Nanomaterials and Their Application in Biological and Chemical Sensing. *Chem. Rev.* **2010**, *110*, 5332.

(3) Pradhan, N.; Pal, A.; Pal, T. Catalytic Reduction of Aromatic Nitro Compounds by Coinage Metal Nanoparticles. *Langmuir* **2001**, *17*, 1800.

(4) Ghosh, S. K.; Mandal, M.; Kundu, S.; Nath, S.; Pal, T. Bimetallic Pt-Ni Nanoparticles Can Catalyze Reduction of Aromatic Nitro Compounds by Sodium Borohydride in Aqueous Solution. *Appl. Catal., A* **2004**, *268*, 61.

(5) Shilcrat, S. Process Safety Evaluation of a Tungsten-Catalyzed Hydrogen Peroxide Epoxidation Resulting in a Runaway Laboratory Reaction. *Org. Process Res. Dev.* **2011**, *15*, 1464.

(6) Kimura, T.; Kamata, K.; Mizuno, N. A Bifunctional Tungstate Catalyst for Chemical Fixation of $CO_2$ at Atmospheric Pressure. *Angew. Chem., Int. Ed.* **2012**, *51*, 6700.

(7) Roy, S.; Bhar, S. Sodium Tungstate-Catalyzed "on-Water" Synthesis of B-Arylvinyl Bromides. *Green Chem. Lett. Rev.* **2010**, *3*, 341.

(8) Shi, M.; Feng, Y. S. Oxidation of Benzyl Chlorides and Bromides to Benzoic Acids with 30 Hydrogen Peroxide in the Presence of $Na_2WO_4$, $Na_2VO_4$, or $Na_2MoO_4$ under Organic Solvent-Free Conditions. *J. Org. Chem.* **2001**, *66*, 3235.

(9) Wu, Y. G.; Wen, M.; Wu, Q. S.; Fang, H. Ni/Graphene Nanostructure and Its Electron-Enhanced Catalytic Action for Hydrogenation Reaction of Nitrophenol. *J. Phys. Chem. C* **2014**, *118*, 6307.

(10) Moussa, S.; Siamaki, A. R.; Gupton, B. F.; El-Shall, M. S. Pd-Partially Reduced Graphene Oxide Catalysts (Pd/PRGO): Laser Synthesis of Pd Nanoparticles Supported on PRGO Nanosheets for Carbon-Carbon Cross Coupling Reactions. *ACS Catal.* **2012**, *2*, 145.

(11) Siamaki, A. R.; Khder, A. E. R. S. K.; Abdelsayed, V.; El-Shall, M. S.; Gupton, B. F. Microwave-Assisted Synthesis of Palladium Nanoparticles Supported on Graphene: A Highly Active and Recyclable Catalyst for Carbon-Carbon Cross-Coupling Reactions. *J. Catal.* **2011**, *279*, 1.

(12) Vaidya, M. J.; Kulkarni, S. M.; Chaudhari, R. V. Synthesis of P-Aminophenol by Catalytic Hydrogenation of P-Nitrophenol. *Org. Process Res. Dev.* **2003**, *7*, 202.

(13) Meng, N.; Zhang, S.; Zhou, Y.; Nie, W.; Chen, P. Novel Synthesis of Silver/Reduced Graphene Oxide Nanocomposite and Its



DOI: 10.1021/acs.iecr.6b01882
*Ind. Eng. Chem. Res.* 2016, 55, 7267−7272

High Catalytic Activity Towards Hydrogenation of 4-Nitrophenol. *RSC Adv.* **2015**, *5*, 70968.
(14) Woo, H.; Kim, J. W.; Kim, M.; Park, S.; Park, K. H. Au Nanoparticles Supported on Magnetically Separable $Fe_2O_3$-Graphene Oxide Hybrid Nanosheets for the Catalytic Reduction of 4-Nitrophenol. *RSC Adv.* **2015**, *5*, 7554.
(15) Rode, C.; Vaidya, M.; Chaudhari, R. Synthesis of P-Aminophenol by Catalytic Hydrogenation of Nitrobenzene. *Org. Process Res. Dev.* **1999**, *3*, 465.
(16) Hummers, W. S., Jr; Offeman, R. E. Preparation of Graphitic Oxide. *J. Am. Chem. Soc.* **1958**, *80*, 1339.
(17) Huang, G.; Shi, R.; Zhu, Y. Photocatalytic Activity and Photoelectric Performance Enhancement for $ZnWO_4$ by Fluorine Substitution. *J. Mol. Catal. A: Chem.* **2011**, *348*, 100.
(18) Rahimi Nasrabadi, M.; Pourmortazavi, S. M.; Ganjali, M. R.; Hajimirsadeghi, S. S.; Zahedi, M. M. Electrosynthesis and Characterization of Zinc Tungstate Nanoparticles. *J. Mol. Struct.* **2013**, *1047*, 31.
(19) Raja, K.; Verma, S.; Karmakar, S.; Kar, S.; Das, S. J.; Bartwal, K. Synthesis and Characterization of Magnetite Nanocrystals. *Cryst. Res. Technol.* **2011**, *46*, 497.
(20) Huang, G.; Zhu, Y. Synthesis and Photocatalytic Performance of $ZnWO_4$ Catalyst. *Mater. Sci. Eng., B* **2007**, *139*, 201.
(21) Nethravathi, C.; Nisha, T.; Ravishankar, N.; Shivakumara, C.; Rajamathi, M. Graphene-Nanocrystalline Metal Sulphide Composites Produced by a One-Pot Reaction Starting from Graphite Oxide. *Carbon* **2009**, *47*, 2054.
(22) Szabó, T.; Berkesi, O.; Dékány, I. Drift Study of Deuterium-Exchanged Graphite Oxide. *Carbon* **2005**, *43*, 3186.
(23) Xu, J.; Chen, M.; Wang, Z. Preparation of $CdWO_4$-Deposited Reduced Graphene Oxide and Its Enhanced Photocatalytic Properties. *Dalton Trans.* **2014**, *43*, 3537.
(24) Wang, H.; Robinson, J. T.; Li, X.; Dai, H. Solvothermal Reduction of Chemically Exfoliated Graphene Sheets. *J. Am. Chem. Soc.* **2009**, *131*, 9910.
(25) Subramanya, B.; Bhat, D. K. Novel One-Pot Green Synthesis of Graphene in Aqueous Medium under Microwave Irradiation Using a Regenerative Catalyst and the Study of Its Electrochemical Properties. *New J. Chem.* **2015**, *39*, 420.
(26) Ahmad, M.; Ahmed, E.; Hong, Z.; Ahmed, W.; Elhissi, A.; Khalid, N. Photocatalytic, Sonocatalytic and Sonophotocatalytic Degradation of Rhodamine B Using ZnO/CNTs Composites Photocatalysts. *Ultrason. Sonochem.* **2014**, *21*, 761.
(27) Cortés Jácome, M.; Angeles Chavez, C.; Lopez Salinas, E.; Navarrete, J.; Toribio, P.; Toledo, J. Migration and Oxidation of Tungsten Species at the Origin of Acidity and Catalytic Activity on $WO_3$-$ZrO_2$ Catalysts. *Appl. Catal., A* **2007**, *318*, 178.
(28) Zhao, X.; Yao, W.; Wu, Y.; Zhang, S.; Yang, H.; Zhu, Y. Fabrication and Photoelectrochemical Properties of Porous $ZnWO_4$ Film. *J. Solid State Chem.* **2006**, *179*, 2562.
(29) Zubir, N. A.; Yacou, C.; Motuzas, J.; Zhang, X.; da Costa, J. C. D. Structural and Functional Investigation of Graphene Oxide-$Fe_3O_4$ Nanocomposites for the Heterogeneous Fenton-Like Reaction. *Sci. Rep.* **2014**, *4*, 4594.
(30) Zheng, J.; Dong, Y.; Wang, W.; Ma, Y.; Hu, J.; Chen, X.; Chen, X. In Situ Loading of Gold Nanoparticles on $Fe_3O_4$@$SiO_2$ Magnetic Nanocomposites and Their High Catalytic Activity. *Nanoscale* **2013**, *5*, 4894.
(31) Islam, D.; Acharya, H. Magnetically Separable Palladium Nanocluster Supported Iron Based Metal-Organic Framework (MIL-88B) Catalyst in Efficient Hydrogenation Reactions. *RSC Adv.* **2015**, *5*, 46583.
(32) Jiang, H. L.; Akita, T.; Ishida, T.; Haruta, M.; Xu, Q. Synergistic Catalysis of Au@Ag Core-Shell Nanoparticles Stabilized on Metal-Organic Framework. *J. Am. Chem. Soc.* **2011**, *133*, 1304.
(33) Li, J.; Liu, C. Y.; Liu, Y. Au/Graphene Hydrogel: Synthesis, Characterization and Its Use for Catalytic Reduction of 4-Nitrophenol. *J. Mater. Chem.* **2012**, *22*, 8426.
(34) Yang, Y.; Ren, Y.; Sun, C.; Hao, S. Facile Route Fabrication of Nickel Based Mesoporous Carbons with High Catalytic Performance Towards 4-Nitrophenol Reduction. *Green Chem.* **2014**, *16*, 2273.


DOI: 10.1021/acs.iecr.6b01882
*Ind. Eng. Chem. Res.* 2016, 55, 7267−7272